



**HAL**  
open science

**Alkaline-earth metal-doped perovskites  
 $\text{La}_{0.95}\text{A}_{0.05}\text{MnO}_{3+\delta}$  (A = Ca, Sr): New structural and  
magnetic features revealed by  $^{57}\text{Fe}$  Mössbauer  
spectroscopy and magnetic measurements**

Diana Pchelina, Vera Sedykh, Nataliya Chistyakova, Vyacheslav Rusakov,  
Yulia Alekhina, Alexey Tselebrovskiy, Bernard Fraisse, Lorenzo Stievano,  
Moulay Tahar Sougrati

► **To cite this version:**

Diana Pchelina, Vera Sedykh, Nataliya Chistyakova, Vyacheslav Rusakov, Yulia Alekhina, et al.. Alkaline-earth metal-doped perovskites  $\text{La}_{0.95}\text{A}_{0.05}\text{MnO}_{3+\delta}$  (A = Ca, Sr): New structural and magnetic features revealed by  $^{57}\text{Fe}$  Mössbauer spectroscopy and magnetic measurements. Journal of Physics and Chemistry of Solids, 2021, 159, pp.110268. 10.1016/j.jpcs.2021.110268 . hal-03293735

**HAL Id: hal-03293735**

**<https://hal.science/hal-03293735>**

Submitted on 21 Jul 2021

**HAL** is a multi-disciplinary open access archive for the deposit and dissemination of scientific research documents, whether they are published or not. The documents may come from teaching and research institutions in France or abroad, or from public or private research centers.

L'archive ouverte pluridisciplinaire **HAL**, est destinée au dépôt et à la diffusion de documents scientifiques de niveau recherche, publiés ou non, émanant des établissements d'enseignement et de recherche français ou étrangers, des laboratoires publics ou privés.

# Alkaline-earth metal-doped perovskites $\text{La}_{0.95}\text{A}_{0.05}\text{MnO}_{3+\delta}$ (A = Ca, Sr): new structural and magnetic features revealed by $^{57}\text{Fe}$ Mössbauer spectroscopy and magnetic measurements

Diana Pchelina<sup>a\*</sup>, Vera Sedykh<sup>b</sup>, Nataliya Chistyakova<sup>a</sup>, Vyacheslav Rusakov<sup>a</sup>, Yulia Alekhina<sup>a</sup>, Alexey Tselebrovskiy<sup>a</sup>, Bernard Fraisse<sup>c</sup>, Lorenzo Stievano<sup>c\*</sup> and Moulay Tahar Sougrati<sup>c</sup>

<sup>a</sup>Lomonosov Moscow State University, Moscow, 119991 Russia

<sup>b</sup>Institute of Solid State Physics, Russian Academy of Sciences, Chernogolovka, 142432 Russia

<sup>c</sup>ICGM, Univ Montpellier, CNRS, ENSCM, Montpellier, France

\*Corresponding author at:

ICGM, Univ. Montpellier, CNRS, Place Eugène Bataillon, Montpellier, 34095, France

Tel. +33 (0) 4 67 14 33 46

E-mail: [lorenzo.stievano@umontpellier.fr](mailto:lorenzo.stievano@umontpellier.fr)

Lomonosov Moscow State University, GSP-1, Leninskie Gory, Moscow, 119991, Russia

Tel. +7 495 9391000

E-mail: [di.pchelina@physics.msu.ru](mailto:di.pchelina@physics.msu.ru),

## Abstract

Ca- and Sr-doped lanthanum manganese perovskites  $\text{La}_{0.95}\text{A}_{0.05}\text{Mn}_{0.98}\text{Fe}_{0.02}\text{O}_{3+\delta}$  (A = Ca, Sr) (LCM and LSM) of non-stoichiometric (NS) and stoichiometric (S) compositions were prepared by sol-gel method and investigated by  $^{57}\text{Fe}$  Mössbauer spectroscopy and magnetic measurements. In contrast to non-stoichiometric samples, which contain pure single phases, a mixture of orthorhombic phases *PnmaI*, *PnmaII* and *PnmaII\** are detected in samples of stoichiometric compositions. The magnetic data, supported by Mössbauer measurements, show the spontaneous formation of magnetically ordered clusters with sizes in the range 2.5-4.6 nm in all samples. The main differences between the investigated LCM and LSM systems, and in particular the less extended phase separation in LSM-S than in LCM-S is connected to the difference in ionic radii on the doping ions, the influence of the Jahn-Teller effect at the  $\text{Mn}^{+3}$  centres and the size distributions of the ferromagnetic clusters. Our results show, for the first time, that the *PnmaII\** phase is characterized by antiferromagnetic ordering.

**Keywords:** perovskites, doped lanthanum manganites, Mössbauer spectroscopy, phase separation, magnetic properties, superparamagnetism.

## 1. Introduction

Doped lanthanum manganites of the  $\text{La}_{1-x}\text{A}_x\text{MnO}_3$ -type (LAM), where A is a divalent alkali-earth metal ion  $\text{Ca}^{2+}$ ,  $\text{Sr}^{2+}$  or  $\text{Ba}^{2+}$ , are widely applied as cathode elements for fuel cells, in information recording and solid-state storage devices, and in the production of hydrogen with solar energy [1–5]. These compounds, largely investigated from both the fundamental and the applied point of view, derive from the parent compound  $\text{LaMnO}_3$  and usually exist in the non-stoichiometric form  $\text{La}_{1-x}\text{A}_x\text{MnO}_{3+\delta}$ . In non-stoichiometric  $\text{LaMnO}_{3+\delta}$ , manganese is contained both as  $\text{Mn}^{+3}$  and  $\text{Mn}^{+4}$ . In the stoichiometric composition, however, manganese is only in the trivalent state, which undergoes Jahn-Teller distortion and leads to severe distortions of the crystal lattice, and eventually to the phase transition from the highly symmetric phase *PnmaI* to low-symmetry *PnmaII* [6]. Below the temperature of magnetic ordering, the paramagnetic phase *PnmaI* and *PnmaII* become ferromagnetic and antiferromagnetic, respectively [7].

The stoichiometric composition ( $\delta = 0$ ) can be obtained in two ways: (i) by introducing increasing amounts of a divalent doping element, which by charge compensation stabilises increasing contents of non-Jahn-Teller  $\text{Mn}^{+4}$  ions, or (ii) by removing interstitial oxygen. Up to now, stoichiometric LAM with low contents ( $x \leq 0.2$ ) of the doping element have been only rarely studied.

Previous investigations of stoichiometric LAM containing low amounts of dopants, carried out at room temperature, revealed structural phase separation correlated with the Jahn-Teller effect [6,7,8]. The strongest differences was observed for a dopant concentration of 5 %, corresponding to a low content of  $\text{Mn}^{4+}$ , which was attributed to the occurrence of competing processes [8,9]. For Ca-doped LAM, this problem was preliminary investigated by Mössbauer spectroscopy at 5 K, 80 K and by magnetization measurements [10]. In this work a special model for processing Mössbauer spectra was proposed, allowing us to better understand the nature of the magnetic clusters as well as the magnetic properties of a new *PnmaII*\* phase. However, these properties have not yet sufficiently understood and need further investigations, which may eventually reveal new properties of these manganite phases.

In this work, we studied stoichiometric (S) and non-stoichiometric (NS) LAM (A = Ca, Sr) containing low contents of doping element (5 %) in a wide temperature range (including low temperature), and in particular investigated the effect of doping on the physical properties. The two systems  $\text{La}_{1-x}\text{A}_x\text{MnO}_{3+\delta}$  (A = Ca, Sr) were compared in order to understand the influence of the nature of the doping element on the structural, electronic and magnetic properties, as well as on cluster formation. For instance, the different

ionic radii of Ca and La produces a more intense Jahn-Teller distortion in Ca-than in Sr-doped LMA, which is expected to have a strong impact on structural and magnetic properties.

Compared to previous studies, this one was carried out using a novel approach including the temperature-dependent measurements of the magnetic susceptibility, of the magnetization in ZFC-FC mode as well as of the  $^{57}\text{Fe}$  Mössbauer spectra, the latter made possible by the inclusion of small amounts of isotopically enriched  $^{57}\text{Fe}$  iron in the materials. This comprehensive study allowed a qualitative and quantitative determination of the magnetic state and the transition temperature of the studied phases, as well as their dependence upon the particle size distribution in the different materials.

## 2. Material and methods

Polycrystalline  $\text{La}_{0.95}\text{A}_{0.05}\text{Mn}_{0.98}\text{Fe}_{0.02}\text{O}_{3+\delta}$  (A = Ca, Sr) samples were prepared by the sol-gel method from lanthanum, isotopically enriched  $^{57}\text{Fe}$ , calcium/strontium nitrates and manganese acetate. The synthesis procedure as well as the (no)-stoichiometry of the synthesised materials were described in detail in previous works [10,11]. Stoichiometric compositions were obtained by annealing the (no)-stoichiometric samples at  $T = 650^\circ\text{C}$  *in vacuo* ( $10^{-3}$  Torr) for 10 – 15 hours.

$^{57}\text{Fe}$  Mössbauer spectra were measured using a  $^{57}\text{Co}$  (Rh) source on an MS-1104Em spectrometer at 300 and 80 K, and a WissEl spectrometer equipped with a Janis SHI-850 cryostat for low-temperature analyses below 80 K. The spectra were processed using the SpectrRelax computer program [12] using the many-state superparamagnetic relaxation model. Within this model, the parameter  $\alpha$  is the ratio of the magnetic-anisotropy energy to the thermal-oscillation energy:  $\alpha = \frac{K_{\text{eff}}V}{k_B T}$  ( $K_{\text{eff}}$  is effective magnetic anisotropy constant,  $V$  – the particle volume,  $k_B$  – the Boltzmann constant,  $T$  – the absolute temperature).

Magnetization measurements were carried out on a LakeShore 7404 vibrating sample magnetometer in the temperature range 100-300 K in fields up to 1280 kA/m. Investigations of the temperature dependence of the magnetization in ZFC-FC mode (heating in a nonzero field after cooling in a zero magnetic field (ZFC - Zero-Field Cooled) and cooling in a non-zero field (FC - Field Cooling)) in an external magnetic field of 2.4 kA/m (30 Oe) were carried out in the temperature range 100-300 K. Magnetic ZFC-FC measurements in the range 2–300 K with the magnetic field up to 5 Tesla (in an external magnetic field of 8 kA/m or 100 Oe) were collected with a Quantum Design MPMS-7XL SQUID magnetometer.

The temperature dependence of the magnetic susceptibility was measured on an AGICO Kappabridges MFK1-A instrument in the temperature range 70-275 K. The sensitivity of the device is  $1 * 10^{-7}$  SI. The Néel temperature  $T_N$  was estimated from the temperature dependence of the magnetic susceptibility. The Curie-Weiss temperature  $\Theta_{\text{CW}}$  was determined by linear extrapolation from the  $1/\chi$  vs. temperature experimental plot.

In order to calculate the size of the magnetic clusters from the magnetic measurements, the magnetization curve was approximated by a linear function in the saturation region, In this way, the reference parameters of the saturation magnetization and the paramagnetic contribution coefficient  $A$  were determined. Then, a section of the magnetization curve where the magnetization is not less than 90% of the obtained saturation magnetization was selected. This section was approximated by the magnetization

function  $M(H)$ , approximated for all the studied samples by the function  $\frac{M(H)}{M_s} = 1 - \left(\frac{2aK_{eff}}{M_s H}\right)^2$ . Here  $M_s$  is saturation magnetization,  $a$  is symmetry parameter, describing the special distribution of easy magnetization axes,  $K_{eff}$  is the effective anisotropy constant,  $H$  is magnetic field. The effective anisotropy constant at a temperature below the blocking temperature was estimated using the Akulov's law [13]. To subtract the paramagnetic contribution, the linear field term was added. Thus, the function was used in the form  $M(H) = M_s + A * H - \frac{B}{M_s} * \frac{1}{H^2}$ , with  $A$  and  $B$  as fitting parameters. The effective anisotropy constant was determined from parameter  $B$ . The symmetry parameter  $a$  was taken equal to 0.5, which corresponds to systems with a random distribution of the axes of easy magnetization. Then the values of  $K_{eff}$ , reported in Table 4, are determined as  $B = K_{eff}^2$ .

### 3. Results and discussion

#### 3.1. Crystal structure of the studied materials

The crystal structure of all samples was determined by X-ray diffraction (XRD) in previous works [10,11,14]. The LCM-NS and LSM-NS samples studied in this work are rhombohedral (space group  $R\bar{3}c$ ). The LCM-S and LSM-S samples obtained by annealing in vacuo the respective LAM-NS precursors have an orthorhombic  $PnmaII^*$  structure (space group  $Pnma$ ). The lattice parameters for all samples are listed in Table 1 and compared to those of the parent compound  $\text{LaMnO}_{3+\delta}$ . These data clearly show that 5 % doping is sufficient to produce significant structural changes in systems of stoichiometric composition. The emergence of  $\text{Mn}^{4+}$  leads to a structural change: the  $PnmaII$  phase begins to transform into the high symmetry  $PnmaI$  phase via the  $PnmaII^*$  intermediate. One should note that it is difficult to discriminate the three orthorhombic phases by XRD in a mixture of stoichiometric low-doping LAM since their patterns are very close to each other [14].

#### 3.2. $^{57}\text{Fe}$ Mössbauer spectroscopy analysis

The small amount of isotopically-enriched  $^{57}\text{Fe}$  added to perform the Mössbauer spectroscopy analysis is known to replace  $\text{Mn}^{3+}$  in the crystal structure as  $\text{Fe}^{3+}$  [6]. Since the ionic radii of  $\text{Fe}^{3+}$  and  $\text{Mn}^{3+}$  are very similar, Fe-doping practically does not introduce any distortion in the lattice, and, according to XRD, the lattice parameters are not modified with such low Fe loadings [6,15]. However, as previously shown in

refs. [6,10,11,15], even a small iron loading in undoped stoichiometric lanthanum manganite leads to phase separation: in addition to the main contribution of the *PnmaII* phase in the XRD pattern, small amounts of two other orthorhombic phases *PnmaII\** and *Pnmal* can be identified. This means that, similarly to  $\text{Mn}^{4+}$ , also  $\text{Fe}^{3+}$  destroys the Jahn-Teller distortion as expected given its  $d^5$  electron configuration.

The Mössbauer spectra at 300 and 80 K of samples LCM-NS, already studied in refs. [16,17], and LSM-NS are shown in Fig. 1, and the corresponding hyperfine parameters are presented in Table 2. The spectra at room temperature consist of an asymmetric quadrupole contribution, indicating the (super)paramagnetic nature of the pristine samples. The spectra were processed using distributions of quadrupole splitting. The local environments of iron nuclei with the parameters of the Mössbauer spectra shown in Table 2 correspond to the *R-3c* phase. The maximum isomer shift values  $\delta_{\text{max}}$  are almost identical for all spectra and are characteristic of high spin trivalent iron located in octahedral oxide environments. The maximum quadrupole splitting ( $\Delta$ ) of the *R-3c* phase is larger in the spectrum of the LCM-NS sample than in LSM-NS. This result reflects a lower distortion of the local environment of the Fe centres in LSM-NS compared to LCM-NS, which can be attributed to a smaller amount of interstitial oxygen. This probably derives from the smaller ionic radius of  $\text{Ca}^{2+}$  compared to  $\text{Sr}^{2+}$  and  $\text{La}^{3+}$ , which leads to a smaller unit cell volume for LCM-NS [11].

The LSM-NS sample spectrum at 80 K (Figure 1d) is a broadened sextet with a typical shape of relaxation spectra; for the LCM-NS sample, it is a combination of a broadened sextet and a quadrupole doublet, the later representing approximately 25% of the total absorption [16]. The spectrum of the LSM-NS sample was fitted using a distribution of hyperfine magnetic fields as implemented in the model of many-state superparamagnetic relaxation [18]. The shape of the spectra is characteristic of small magnetic particles heterogeneous in size undergoing superparamagnetic relaxation, leading to a distribution of hyperfine magnetic fields, as previously shown in for LCM-NS [16]. For LSM-NS,  $T_b$  lies above 80 K. An additional quadrupole doublet in LCM-NS is due to the presence of tiny magnetic clusters having a blocking temperature below 80 K. This was previously confirmed for LCM-NS, which Mössbauer spectrum at 5 K shows only a magnetic contribution [16].

The Mössbauer spectra of the stoichiometric ( $\delta = 0$ ) samples LCM-S and LSM-S obtained by vacuum annealing, measured at 300 K, are shown in Fig. 2. The spectra were first processed using distributions of

quadrupole splittings, which permitted us to determine the number of spectral components in the samples as well as their respective contributions. The spectra of LCM-S and LSM-S were then fitted by a combination of three and two quadrupole doublets, respectively (Table 3).

According to previous investigations [9], each subspectrum should correspond to a specific orthorhombic phase: on going from the smallest to the largest quadrupole splitting, subspectra 1, 2 and 3 should then represent the increasingly distorted phases *PnmaI*, *PnmaII\** and *PnmaII*. In this hypothesis, LCM-S contains the three phases, whereas in LSM-S no trace of the *PnmaI* phase is found. In these samples, the evolution of the different phases can be related to the oxidation state of the manganese centres: the *PnmaII* phase, containing in only Jahn-Teller  $Mn^{3+}$  ions, has a strongly distorted lattice. Doping with a divalent impurity induces the partial replacement of the  $Mn^{3+}$  ions by non-Jahn-Teller  $Mn^{4+}$ , leading to the transformation of the *PnmaII* phase transforms in the more symmetric *PnmaI* one. The relative intensity of each subspectrum, which can be considered as a measure of the relative concentration of each phase if their Lamb-Mössbauer factors are assumed to be equal, are different for LCM-S and LSM-S (cf. Table 3). The prevailing contribution of the *PnmaII* phase in LCM-S can be related to the difference in ionic radii of the doping elements and lanthanum, as already described in refs. [8,9].

The Mössbauer spectra of LCM-S and LSM-S at 80 K (cf. Fig. 2) show only a relatively broad magnetic contribution, which can be fitted with 3 and 2 components (cf. Table 3), respectively, in line with the fits of the room temperature spectra: a distribution of magnetic fields and two relaxation subspectra in many-state superparamagnetic relaxation model [18] were used for LCM-S, whereas a distribution of the magnetic fields and one relaxation sextet were used for LSM-S. As for the nonstoichiometric samples, the relaxation components are connected with the presence of superparamagnetic particles [9,16,17]. By the analogy with previous work [9], we can assume that at low temperature the magnetic hyperfine field decreases in the series *PnmaI* > *PnmaII\** > *PnmaII*.

In conclusion, Mössbauer spectroscopy shows the formation of a phase-separated system composed of coexisting orthorhombic phases in the stoichiometric lanthanum manganites after removing interstitial oxygen by vacuum annealing. Different amounts of the different phases are found in LSM-S compared to LCM-S due to the different ionic radii of the dopant ions. The undergoing of superparamagnetic relaxation is proved by the temperature dependence of the Mössbauer spectra, and is attributed to the

presence of magnetic nanoparticles. The lower relaxation rate of the *PnmaI* phase can be related to the presence of particles of larger sizes than for the other phases.

### 3.3. Magnetic measurements

#### 3.3.1. Magnetostatic measurements

Magnetic measurements were carried out to better understand the effect of doping and stoichiometry on the physical properties. In agreement with Mössbauer spectroscopy, both stoichiometric and non-stoichiometric samples exhibit paramagnetic behaviour at 300 K (Fig. 3), while magnetic order is reached at 100 K for all samples (Fig. 4). As expected, stoichiometric samples showed much lower magnetization values in the maximum field compared to non-stoichiometric ones. An increase in the coercive field for stoichiometric samples (more than 5 times that of non-stoichiometric samples) indicates the appearance of magnetic anisotropy. Anisotropy can be caused by the appearance of a higher coercive phase or by an increase in cluster size after the temperature treatment of the samples. Moreover, the shape of the hysteresis loops (lack of saturation and the loop shift) of the annealed samples indicates the presence of an antiferromagnetic phase in their composition (Fig. 4). Saturation is not achieved for the LCM-S sample in a maximum field of 1280 kA/m; whereas an offset from zero magnetic field is observed indicating the presence of interacting antiferromagnetic and ferromagnetic phases (exchange bias) [19]. The arising of a highly anisotropic antiferromagnetic phase interacting with ferromagnetic clusters leads to the appearance of a wider hysteresis loop. Since the ferromagnetic phase is responsible for the hysteresis, the interaction of ferromagnetic clusters with the antiferromagnetic phase leads to the induction of a kind of anisotropy – a preferred direction of magnetization appears. The consequence of this is an increase in the coercive force and exchange displacement.

#### 3.3.2. Calculation and analysis of the magnetic cluster size from Mössbauer and magnetic measurements

The values of the effective anisotropy constant  $K_{\text{eff}}$  at 100 K reported in Table 4 is very similar for all samples (from 5.5 to  $23 \cdot 10^4 \text{ J/m}^3$ ), suggesting that the cluster sizes depend on the type of doping element

(there is no saturation for the LCM-S; therefore, it was not possible to determine the magnetic anisotropy constant for this sample).

The cluster sizes of LCM and LSM samples of both stoichiometric and non-stoichiometric composition was estimated using a variable parameter  $\alpha$  obtained from Mössbauer spectrum fitting in many-state superparamagnetic relaxation model at 80 K. It follows that cluster sizes in the LCM-NS sample are approximately 1.5 times smaller than in LSM-NS. According to LSM-S we can see that  $PnmaII^*$  phase is characterized by a much larger size of the magnetic clusters region. It can be assumed from an analysis of the data obtained that there is a spontaneous formation of localized magnetic clusters  $\sim 2.5$ - $4.6$  nm above  $T_c$  for all samples. The existence of analogous clusters  $\sim 1.2$  nm in size in doped lanthanum-manganite systems was detected using small-angle neutron scattering measurements in [20].

### 3.3.3. Temperature dependence of the magnetic properties

The temperature dependence of the magnetization in samples LCM-NS and LSM-NS (Fig. 5a) in the temperature range 80-300 K was measured in a field of 2.4 kA/m, which is expected to be less than the coercive field so that the difference between the blocked and unblocked state is visible. In the case of samples LCM-S and LSM-S (Fig. 5b), the measurements were carried out in an external magnetic field of 8 kA/m in the temperature range 0-300 K. These measurements demonstrate the presence of superparamagnetic clusters in the LSM and LCM systems, in agreement Mössbauer spectroscopy. Moreover, for sample LCM-NS, the blocking temperature is outside the measurement range, i.e., below the temperature of liquid nitrogen, also in agreement with the Mössbauer results indicating a large contribution of the disordered phase at 80 K. Such a significant difference in blocking temperatures for the non-stoichiometric samples can also be related to the different size of the ferromagnetic clusters. For samples LCM-S and LSM-S, on the other hand, practically identical blocking temperatures of 120 and 122 K were measured, respectively. Some blurring of the ZFC peak for sample LCM-S indicates a relatively large particle size distribution.

### 3.3.4. Magnetic susceptibility

For all samples, the evolution of the magnetic susceptibility with the temperature was measured, the direct and inverse dependences of which are shown in Fig.6. The measurements were carried between 70

and 275 K. At room temperature, the LCM-NS and LSM-NS samples behave as single-phase paramagnets, while a phase transition to the ferromagnetic state is observed as temperature decreases. The Curie temperatures  $T_c$  corresponding to the initial state of the samples, determined at the intersection of the straight line approximating the linear portion of the reciprocal susceptibility with the abscissa, is higher for LCM-NS than for LSM-NS. It should be noted that, unlike LCM-NS, the LSM-NS sample has a rather sharp drop in susceptibility in the range  $T = 170-185$  K. (Fig.6) This form of the  $\chi(T)$  dependence is typical for characteristic of polycrystalline  $\text{LaMnO}_{3+\delta}$  containing interstitial oxygen [21]. In turn,  $\chi(T)$  for LCM-NS has a more complex form with a singularity in the range 170-230 K. Such behaviour of LCM-NS sample might depend on the presence of small-size magnetic clusters with a transition temperature below 80 K, as confirmed by both Mössbauer and magnetisation results.

Other factors influence the shape of the temperature dependence of the magnetic susceptibility, such as the ionic radius of the dopant. In fact, doping with calcium decreases the volume of the crystal lattice and the amount of interstitial oxygen compared to Sr, which has almost the same size of La. The higher amount of interstitial oxygen in LSM-NS than in LCM-NS induces an increase in number and inhomogeneous distribution of lattice defects, resulting in an inhomogeneous magnetic state. Similarly, the large size distribution of the ferromagnetic nanoparticles in LCM-NS leads to a noticeable increase in  $T_C$  and to a broader phase transition range. Finally, according to iodometric titration, the amount of  $\text{Mn}^{4+}$  ions in LCM-NS is lower than in LSM-NS. Considering the higher magnetic moments of  $\text{Mn}^{3+}$  ( $2 \mu_B$ ) compared to  $\text{Mn}^{4+}$  ( $1.5 \mu_B$ ), a higher effective magnetic moment per cell is expected for LCM-NS. In doped lanthanum manganites, the magnetic order is determined by the sum of contributions from the double exchange  $\text{Mn}^{3+}-\text{O}-\text{Mn}^{4+}$  (DE model) and super-exchange (SE mechanism). The DE model leads to the ferromagnetic ordering of the magnetic moments of Mn ions, and the SE mechanism leads to antiferromagnetic ordering of the magnetic moments of the Fe and Mn ions [22]. Since the Fe content in the two systems is the same and amounts to 2%, it can be assumed that the formation of a Fe-O-Fe bond at such a concentration is unlikely [23], and the only possible metal-oxygen Fe-O-Mn bond occurs via SE mechanism. Also, it can be proposed that the greatest effect will be exerted by double exchange interaction (ferromagnetic ordering always creates a greater magnetic moment than antiferromagnetic ordering). Thus, it can be supposed that the broadening of the transition range to the magnetically ordered

state of the LCM-NS sample over the temperature region (Fig.6 –  $\chi(T)$  slope for (b) is less than for (a)) is associated precisely with a smaller amount of  $Mn^{4+}$  ions than in LSM-NS.

To clarify the nature of magnetic transitions in stoichiometric samples after annealing in vacuum (i.e., in the absence of interstitial oxygen), the dependence of the magnetic susceptibility of LCM-S and LSM-S was measured in similar conditions. Supposing that LCM-S consist of three phases (*PnmaI*, *PnmaII\**, *PnmaII*) and LSM-S of two phases (*PnmaII\**, *PnmaII*), with decreasing temperature, *PnmaI* would transform into a ferromagnetic state, and *PnmaII* into an antiferromagnetic state. For the two samples, therefore, both Néel and the Curie temperatures ( $T_N$  and  $T_c$ , respectively) were determined (cf. Table 5). The first difference between the systems in the form of the  $\chi(T)$  dependence is the different peak widths. The broad peak for sample LCM-S can be explained by the presence of two phases with mismatched Néel temperatures:  $T_{N1}=121$  K,  $T_{N2}=130$  K. In the LSM-S sample, the peak is rather narrow, and it can be at best attributed to two peaks with close Néel temperatures. The second difference is the presence of a detectable ferromagnetic phase for LCM-S with a Curie temperature of about 136 K.

Summarizing the data obtained, we can conclude that the type of alloying element, the amount of interstitial oxygen, and, the number of  $Mn^{4+}$  atoms in samples of nonstoichiometric composition are significant factors affecting the magnetic properties of doped lanthanum manganites. Samples of stoichiometric composition are characterized by the presence of several phases for each of the samples. The results of magnetic studies demonstrate the antiferromagnetic behaviour of LSM-S, which allows us to conclude that the magnetic order in *PnmaII\** is antiferromagnetic. Magnetic measurements confirm the coexistence of several phases characterized by different magnetic ordering.

## 4. Conclusion

Attractive structural and magnetic properties are manifested precisely in low-doped lanthanum manganites by virtue of presence of different interactions: Jahn-Teller effect, double and super-exchange, coexistence of antiferromagnetic and ferromagnetic order.

Here, via the complementary information obtained by Mössbauer spectroscopy, magnetization and magnetic susceptibility measurements, it is shown that the type of doping element, i.e., Ca or Sr, the amount of interstitial oxygen, as well as the change in the  $Mn^{3+}/Mn^{4+}$  ratio lead to intrinsic inhomogeneities and the coexistence of varying amounts of different structural and magnetic phases. Different orthorhombic structures, which were practically impossible to distinguish by X-ray diffraction methods, could thus be evidenced. In addition, it is shown for the first time that the *PnmaII\** phase is characterized by antiferromagnetic ordering.

The presence of superparamagnetic clusters with more or less wide distribution of sizes depending on the composition could be demonstrated by the temperature dependence of the Mossbauer spectra and the magnetization curves measured with an external field. The *PnmaII\** phase, in particular, is characterized by a much larger sizes. The presence of such clusters can be considered as a proof of the high stability of ferromagnetic ordering.

## **Declaration of interests**

The authors declare that they have no known competing financial interests or personal relationships that could have appeared to influence the work reported in this paper.

## **Acknowledgments**

The authors thank C. Reibel (PAC-ICGM, Univ. Montpellier), for magnetic measurements and N.S. Perov (Lomonosov Moscow State University) for discussing the results of magnetic measurements.

The reported study was funded by RFBR, project number 19-32-90222.

## Referenses

- [1] S.S.P. Parkin, Giant Magnetoresistance in Magnetic Nanostructures, *Annu. Rev. Mater. Sci.* 25 (1995) 357–388. doi:10.1146/annurev.ms.25.080195.002041.
- [2] V. V. Kharton, A.P. Viskup, E.N. Naumovich, V.N. Tikhonovich, Oxygen permeability of  $\text{LaFe}_{1-x}\text{Ni}_x\text{O}_{3-\delta}$  solid solutions, *Mater. Res. Bull.* 34 (1999) 1311–1317. doi:10.1016/S0025-5408(99)00117-8.
- [3] K. Huang, J. Wan, J.B. Goodenough, Oxide-ion conducting ceramics for solid oxide fuel cells, *J. Mater. Sci.* 36 (2001) 1093–1098. doi:10.1023/A:1004813305237.
- [4] N. Gokon, K. Hara, Y. Sugiyama, S. Bellan, T. Kodama, C. Hyun-seok, Thermochemical two-step water splitting cycle using perovskite oxides based on  $\text{LaSrMnO}_3$  redox system for solar  $\text{H}_2$  production, *Thermochim. Acta.* 680 (2019) 178374. doi:10.1016/j.tca.2019.178374.
- [5] S.P. Jiang, Development of lanthanum strontium manganite perovskite cathode materials of solid oxide fuel cells: a review, *J. Mater. Sci.* 43 (2008) 6799–6833. doi:10.1007/s10853-008-2966-6.
- [6] V. Sedykh, V.S. Shekhtman, I.I. Zverkova, A.V. Dubovitskii, V.I. Kulakov, Reversibility of structure phase transitions in  $\text{LaMnO}_{3+\delta}$  manganite under heat treatment, *Phys. C Supercond.* 433 (2006) 189–194. doi:10.1016/j.physc.2005.10.013.
- [7] Q. Huang, A. Santoro, J. Lynn, Structure and magnetic order in undoped lanthanum manganite, *Phys. Rev. B - Condens. Matter Mater. Phys.* 55 (1997) 14987–14999. doi:10.1103/PhysRevB.55.14987.
- [8] S.F. Dubinin, A. V. Korolev, S.G. Teploukhov, V.E. Arkhipov, É.A. Neïfeld, V.D. Parkhomenko, N.A. Ugryumova, Phase separation in a manganite  $\text{La}_{0.95}\text{Ba}_{0.05}\text{MnO}_3$  crystal, *Phys. Solid State.* 50 (2008) 71–78. doi:10.1134/s1063783408010149.
- [9] D.I. Pchelina, I.Y. Medvetskaya, N.I. Chistyakova, V.S. Rusakov, V.D. Sedykh, Y.A. Alekhina, Mössbauer and Magnetic Studies of Doped Lanthanum Manganite  $\text{La}_{1-x}\text{Ca}_x\text{Mn}_{0.98}\text{Fe}_{0.02}\text{O}_3$  ( $x = 0.05, 0.10, 0.20$ ): II. Stoichiometric Composition and Phase Segregation, *J. Surf. Investig.* 13 (2019) 462–468. doi:10.1134/S1027451019030303.
- [10] V.D. Sedykh, I.I. Zver'kova, V.S. Shekhtman, A. V. Dubovitskiĭ, V.I. Kulakov, Mössbauer and X-ray studies of the structural phase transformations and suppression of polymorphism in  $\text{La}_{1-x}\text{Sr}_x\text{Mn}_{0.98}\text{Fe}_{0.02}\text{O}_3 + \delta$  ( $x = 0.05-0.30$ ), *Phys. Solid State.* 52 (2010) 591–598.

doi:10.1134/S1063783410030212.

- [11] V.D. Sedykh, V.S. Rusakov, I.I. Zver'kova, A. V. Dubovitskii, V.I. Kulakov, Specific features of the structural transformations in  $\text{La}_{1-x}\text{Ca}_x\text{Mn}_{0.98}\text{Fe}_{0.02}\text{O}_3 + \delta$  ( $x = 0.05\text{--}0.50$ ), *Phys. Solid State*. 53 (2011) 1440–1447. doi:10.1134/S1063783411070237.
- [12] M.E. Matsnev, V.S. Rusakov, SpectrRelax: An application for Mössbauer spectra modeling and fitting, in: *AIP Conf. Proc.*, American Institute of Physics AIP, 2012: pp. 178–185. doi:10.1063/1.4759488.
- [13] N.S. Akulov, Über den Verlauf der Magnetisierungskurve in starken Feldern, *Z. Phys.* 69 (1931) 822–831. doi:10.1007/BF01339465.
- [14] V.D. Sedykh, The features of structural transformations in lanthanum manganites  $\text{La}_{1-x}\text{A}_x\text{MnO}_3 + \delta$  ( $\text{A} = \text{Ca}, \text{Sr}, \text{Ba}$ ), in: *AIP Conf. Proc.*, American Institute of Physics Inc., 2014: pp. 72–80. doi:10.1063/1.4898613.
- [15] V.D. Sedykh, V.S. Shekhtman, A. V. Dubovitskiĭ, I.I. Zver'kova, V.I. Kulakov, Mössbauer and X-Ray studies of the dynamics of phase transformations and suppression of polymorphism in the  $\text{LaMn}_{1-x}\text{Fe}_x\text{O}_3 + \delta$  compound ( $x = 0.015\text{--}0.500$ ), *Phys. Solid State*. 51 (2009) 373–380. doi:10.1134/S1063783409020280.
- [16] D.I. Pchelina, I.Y. Medvetskaya, N.I. Chistyakova, V.S. Rusakov, V.D. Sedykh, Y.A. Alekhina, Mössbauer and Magnetic Studies of Doped Lanthanum Manganite  $\text{La}_{1-x}\text{Ca}_x\text{Mn}_{0.98}\text{Fe}_{0.02}\text{O}_3 + \delta$  ( $x = 0.05, 0.10, 0.20$ ): I. Nonstoichiometric Composition, *J. Surf. Investig. X-Ray, Synchrotron Neutron Tech.* 12 (2018) 1047–1051. doi:10.1134/S1027451018050476.
- [17] V.D. Sedykh, I.Y. Medvetskaya, D.I. Pchelina, N.I. Chistyakova, V.S. Rusakov, Y.A. Alekhina, Mössbauer and Magnetic Study of Lanthanum Manganite  $\text{La}_{1-x}\text{Ca}_x\text{Mn}_{0.98}\text{Fe}_{0.02}\text{O}_3 + \delta$  ( $x = 0.05, 0.10, 0.20$ ): Nonstoichiometric and Stoichiometric Composition, *Crystallogr. Reports*. 65 (2020) 347–351. doi:10.1134/S1063774520030293.
- [18] D.H. Jones, K.K.P. Srivastava, Many-state relaxation model for the Mössbauer spectra of superparamagnets, *Phys. Rev. B*. 34 (1986) 7542–7548. doi:10.1103/PhysRevB.34.7542.
- [19] W.H. Meiklejohn, C.P. Bean, New Magnetic Anisotropy, *Phys. Rev.* 102 (1956) 1413–1414. doi:10.1103/PhysRev.102.1413.
- [20] J.M. De Teresa, M.R. Ibarra, P.A. Algarabel, C. Ritter, C. Marquina, J. Blasco, J. García, A. del

- Moral, Z. Arnold, Evidence for magnetic polarons in the magnetoresistive perovskites, *Nature*. 386 (1997) 256–259. doi:10.1038/386256a0.
- [21] T.I. Arbuzova, B.A. Gizhevskii, R.G. Zakharov, S.A. Petrova, N.M. Chebotaev, Magnetic susceptibility of nanostructural manganite  $\text{LaMnO}_3 + \delta$  produced by mechanochemistry method, *Phys. Solid State*. 50 (2008) 1487–1494. doi:10.1134/S1063783408080179.
- [22] E. Dagotto, *Nanoscale Phase Separation and Colossal Magnetoresistance*, Springer Berlin Heidelberg, Berlin, Heidelberg, 2003. doi:10.1007/978-3-662-05244-0.
- [23] H. Song, W. Kim, S.-J. Kwon, J. Kang, Magnetic and electronic properties of transition-metal-substituted perovskite manganites— $\text{La}_{0.7}\text{Ca}_{0.3}\text{Mn}_{0.95}\text{X}_{0.05}\text{O}_3$  (X=Fe,Co,Ni), *J. Appl. Phys.* 89 (2001) 3398–3402. doi:10.1063/1.1350417.

## Figure Captions

Fig. 1.  $^{57}\text{Fe}$  Mössbauer spectra of LCM-NS and LSM-NS measured at room temperature and 80 K (a,b and c,d, respectively).

Fig. 2.  $^{57}\text{Fe}$  Mössbauer spectra of LCM-S and LSM-S measured at room temperature and 80K (a,b and c,d, respectively).

Fig. 3. Hysteresis loops obtained at 300 K for all samples: 1 – LSM-S, 2 – LSM-NS, 3 – LCM-S, 4 – LCM-NS.

Fig. 4. Hysteresis loops obtained at 100 K for all samples: 1 – LSM-S, 2 – LSM-NS, 3 – LCM-S, 4 – LCM-NS.

Fig. 5. The temperature dependence of the magnetization (ZFC/FC measurements) in the field of 2.4 kA/m for 2-LSM-NS and 4-LCM-NS samples (a) and in the field of 8 kA/m for 1-LSM-S and 3-LCM-S samples (b).

Fig. 6. Temperature dependence of the direct and inverse magnetic susceptibility of the investigated samples: a) LCM-NS, b) LSM-NS, c) LCM-S, d) LSM-S.

## Tables

Table 1. The lattice parameters for the  $R-3c$  and  $PnmaII^*$  phases of  $La_{0.95}A_{0.05}Mn_{0.98}Fe_{0.02}O_{3+\delta}$  ( $A = Sr, Ca$ ) of non-stoichiometric and stoichiometric compositions [14]. For comparison, the data for  $R-3c$  and  $PnmaII$  phases of the parent  $LaMnO_{3+\delta}$  with 1.5 at%  $^{57}Fe$  Mossbauer isotope are listed as well.

Sample	Phase	$a, \text{Å}$	$b, \text{Å}$	$c, \text{Å}$	$V, \text{Å}^3$
$LaMnO_{3+\delta}$	$R-3c$	5.523(2)	-	13.326(4)	352.1(3)
LCM-NS	$R-3c$	5.519(2)	-	13.322(4)	351.4(3)
LSM-NS	$R-3c$	5.522(2)	-	13.343(4)	352.4(3)
$LaMnO_3$	$PnmaII$	5.725(2)	7.703(3)	5.537(2)	244.5(3)
LCM-S	$PnmaII^*$	5.681(2)	7.718(3)	5.534(2)	242.9(3)
LSM-S	$PnmaII^*$	5.638(2)	7.729(3)	5.542(2)	241.8(3)

Table 2. Parameters of the  $^{57}Fe$  Mössbauer spectra of nonstoichiometric  $La_{0.95}A_{0.05}Mn_{0.98}Fe_{0.02}O_{3+\delta}$  ( $A = Ca, Sr$ ) samples measured at room temperature (300 K) and at 80 K.  $\delta$  – is the isomer shift relative to  $\alpha$ -Fe at room temperature,  $\Delta$  – is the quadrupole splitting,  $\Gamma$  – is the width of the Mössbauer line,  $\varepsilon$  – is the quadrupole shift,  $H_n$  – is the hyperfine magnetic field,  $\alpha$  – is the parameter of the relaxation model. The maximum spectral parameters are given for LCM-NS (at RT), LSM-NS.

	Sample	LCM-NS		LSM-NS	
	$T, K$	300	80	300	80
Doublet	$\delta, \text{mm/s}$	0.365±0.001	0.415±0.003	0.366±0.002	-
	$\Delta, \text{mm/s}$	0.290±0.006	0.375±0.005	0.276±0.006	-
	$\Gamma, \text{mm/s}$	0.291±0.018	0.407±0.011	0.250-fix	
Sextet	$\delta, \text{mm/s}$	-	0.496±0.011	-	0.504±0.021
	$\varepsilon, \text{mm/s}$	-	0.043±0.011	-	0.017±0.019
	$\Gamma, \text{mm/s}$	-	0.328±0.030	-	0.250-fix
	$H_n, \text{kOe}$	-	441±3	-	480±6
	$\alpha$	-	1.5±0.1	-	8.1±1.6

Table 3. Parameters of the  $^{57}\text{Fe}$  Mössbauer spectra of stoichiometric  $\text{La}_{0.95}\text{A}_{0.05}\text{Mn}_{0.98}\text{Fe}_{0.02}\text{O}_3$  (A = Ca, Sr) samples measured at room temperature (300 K) and at 80 K.  $\delta$  – is the shift relative to  $\alpha\text{-Fe}$ ,  $\Delta$  – is the quadrupole splitting,  $\Gamma$  – is the width of the Mössbauer line,  $I$  – is the relative intensity of the subspectrum (contribution of each phase),  $H_n$  – is the hyperfine magnetic field,  $\alpha$  – is the parameter of the relaxation model. The maximum spectral parameters are given in the Hamilton model.

	Sample	LCM-S			LSM-S	
	$N_0$ subspectrum	1-( <i>PnmaI</i> )	2-( <i>PnmaII</i> *)	3-( <i>PnmaII</i> )	2-( <i>PnmaII</i> *)	3-( <i>PnmaII</i> )
Doublet $T=300$ K	$\delta$ , mm/s	0.379±0.002	0.379±0.002	0.377±0.001	0.378±0.001	0.377±0.001
	$\Delta$ , mm/s	0.338±0.007	0.782±0.003	1.170±0.001	0.542±0.002	0.857±0.002
	$\Gamma$ , mm/s	0.290±0.002	0.290±0.002	0.290±0.002	0.290±0.010	0.290±0.010
	$I$ , %	9.0±0.4	34.5±0.5	56.5±0.5	54.3±1.1	45.7±1.1%
Sextet $T=80$ K	$\delta$ , mm/s	0.519±0.060	0.609±0.060	0.475±0.010	0.525±0.018	0.491±0.100
	$\Gamma$ , mm/s	0.500 – fix	0.350 – fix	0.250 – fix	0.350 – fix	0.250 – fix
	$H_n$ , kOe	452±7	373 – fix	356.4±0.4	406±2	346±4
	$\alpha$	4±0.1	1±0.1	-	4±0.6	-
	$I$ , %	6.9±1.1	26.0±0.2	67.1±0.1	64.5±8.0	35.5±8.0

Table 4. The parameter  $\alpha$ , calculated in the model of many-state superparamagnetic relaxation for different phases in the samples under study,  $K_{\text{eff}}$  is the calculated magnetic anisotropy constant,  $V$  – the particle volume,  $l$  – approximate clusters size.

		LCM-NS	LSM-NS	LCM-S	LSM-S
$\alpha$	$R-3c$	1.5	10		
	$PnmaI$			4	
	$PnmaII^*$			1	4
$K_{\text{eff}}, J/m^3$		$1.8 \cdot 10^5$	$2.3 \cdot 10^5$	-	$5.5 \cdot 10^4$
$l = \sqrt[3]{V}, nm$	$R-3c$	2.5	3.9		
	$PnmaI$				
	$PnmaII^*$				4.6

Table 5. Blocking temperatures  $T_b$ , the Curie temperatures  $T_C$  and the Néel temperatures  $T_N$  for LSM and LCM samples.

Sample	$T_b, K$ (by maximum of ZFC)	$T_C, K$	$T_N, K$
LCM-S	$120 \pm 2$	$146 \pm 2$	$121 \pm 2; 130 \pm 2$
LCM-NS	$< 100$	$214 \pm 2$	-
LSM-S	$122 \pm 2$	-	range from 122 to 125
LSM-NS	$144 \pm 2$	$186 \pm 2$	-

## Figures

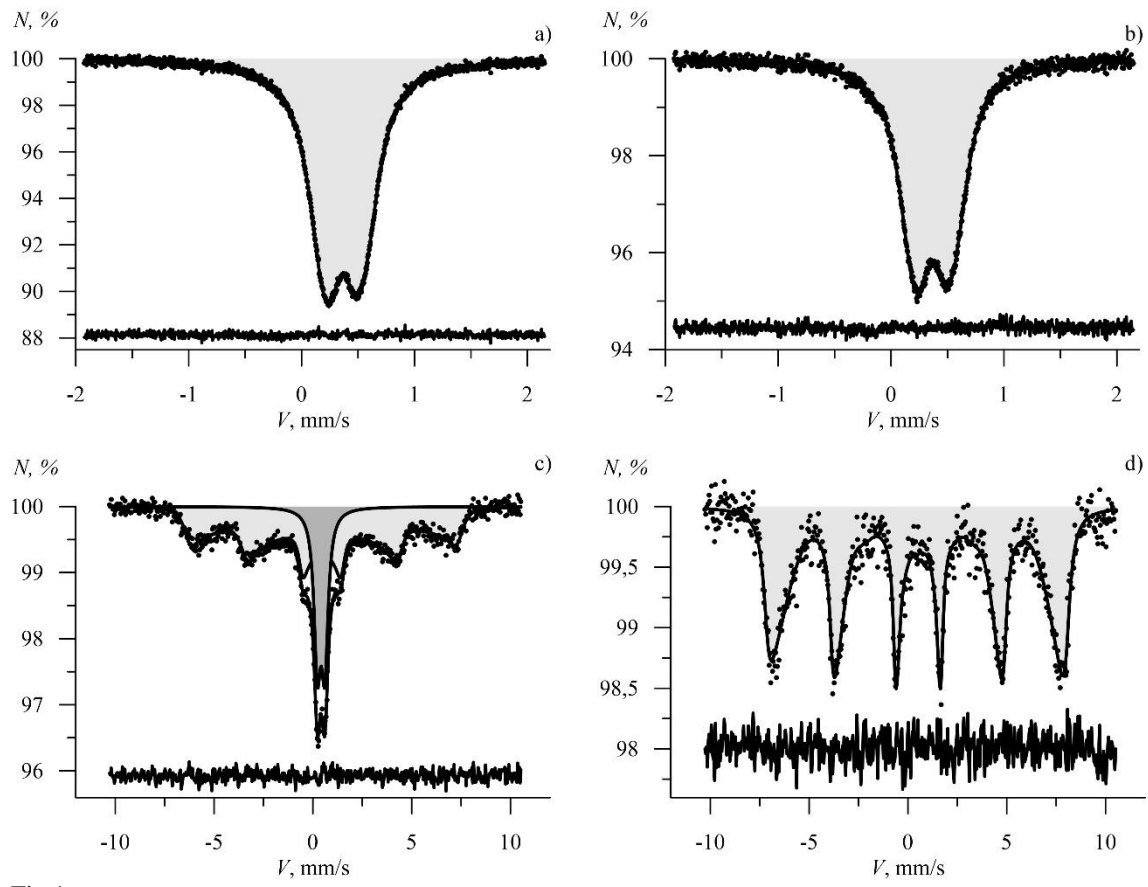


Fig.1.

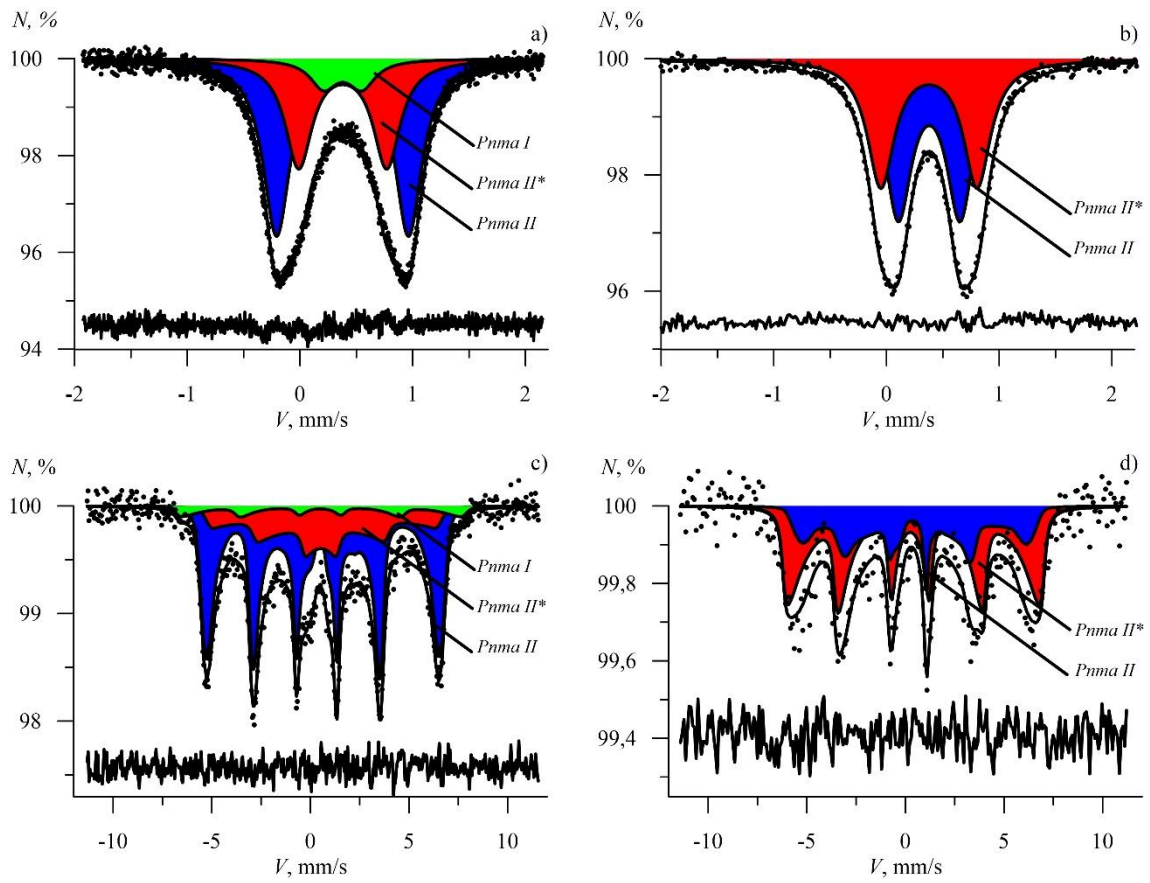


Fig.2.

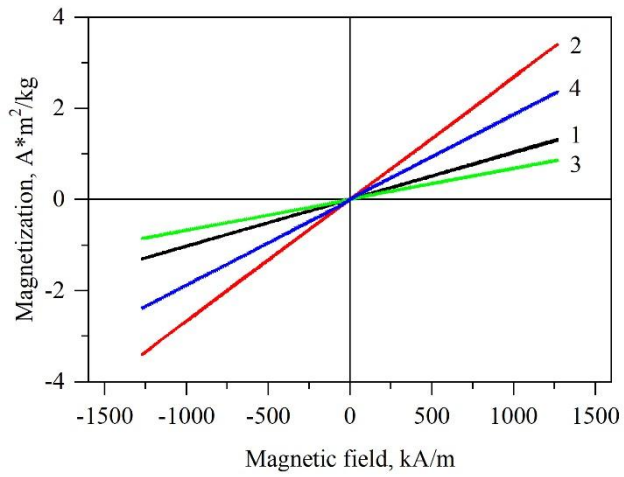


Fig.3.

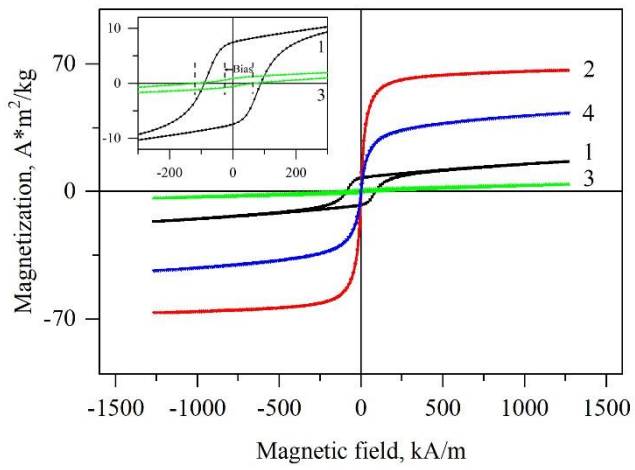


Fig.4.

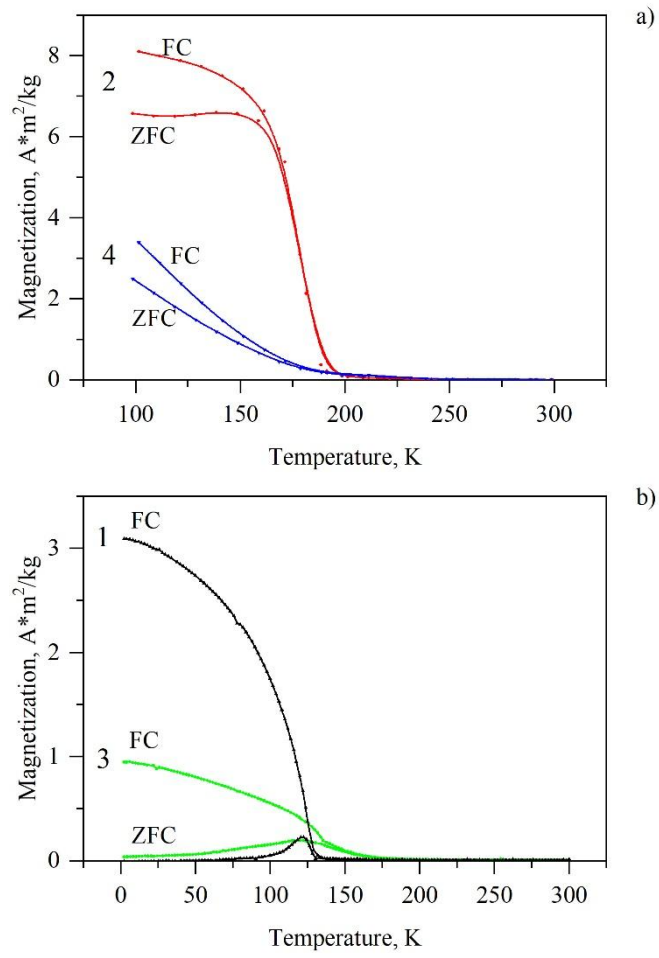


Fig.5.

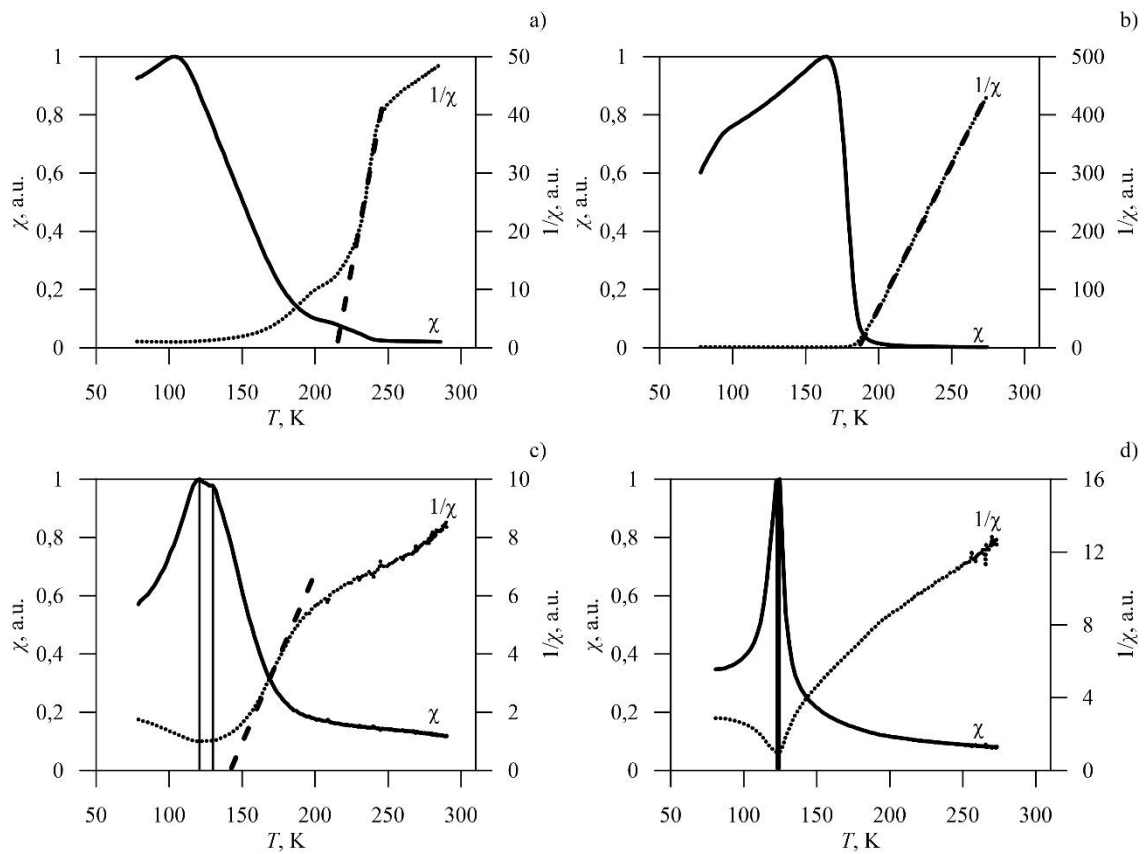


Fig.6.